

VECTOR MESONS IN MEDIUM¹

F. Klingl and W. Weise

*Physik-Department
Technische Universität München
D-85747 Garching, Germany*

Abstract

Based on an effective Lagrangian which combines chiral SU(3) dynamics with vector meson dominance, we have developed a model for the forward vector meson-nucleon scattering amplitudes. We use this as an input to calculate the low energy part of the current-current correlation function in nuclear matter. For the isovector channel we find a significant enhancement of the in-medium spectral density below the ρ resonance while the ρ meson mass itself changes only slightly. The situation is different in the isoscalar channel, where the mass and peak position of the ω meson move downward while its width increases moderately. For the ϕ meson we find almost no mass shift, but the width of the peak increases significantly. We use these spectra as “left hand side” of in medium QCD sum rules and observe a remarkable degree of consistency with the operator product expansion “right hand” side in all three channels. We point out, however, that these results cannot simply be interpreted, as commonly done, in terms of a universal rescaling of vector meson masses in matter. We also compare the resulting thermal dilepton rates of our model with CERES data. We find satisfactory agreement but we point out that the dilepton rates from completely uncorrelated quark-antiquark pairs also fit the data quite well. Considering the strongly attractive potential for the ω together with its comparably small width, we discuss the possible formation of bound ω states in nuclei. Using a Green’s function approach we investigate the possibility of detecting these bound states in the $A(d, {}^3He)$ pick-up reaction.

1 Introduction

It is well known that the chiral symmetry of QCD is spontaneously broken. This leads to the octet of light pseudoscalar mesons which are the Goldstone bosons of this broken symmetry, and to a mass splitting between chiral partners of all hadrons. An example is the vector meson whose chiral partner, the axial vector meson, is twice as heavy. There are, however, strong hints from the quark condensate in medium [1], QCD lattice simulations [2, 3] or

¹Work supported in part by GSI and BMBF

schematic chiral models such as the Nambu-Jona-Lasinio model [4], that this symmetry is expected to be restored at high temperatures and high densities. In order to find some signals for this chiral restoration it was proposed to study dileptons emitted in heavy ion collisions since they can carry information of the inner hot and dense zone of such collisions. Such experiments with high statistics and resolution are planned by the HADES collaboration at GSI. For high temperature there are already data from the CERES [5] and HELIOS [6] collaborations at CERN which observe strongly enhanced dilepton yields below the rho meson resonance. This was often interpreted as an indication of dropping vector meson masses which in addition should be a signal for chiral restoration. The Brown-Rho scaling scenario [7] and considerations based on bag models [8] support this idea and find a strong reduction of the vector mesons masses. Also the QCD sum rule analysis [9], which however only used a delta function caricature of the true spectrum, seemed to confirm these results. From the theoretical point of view chiral restoration, however, does not demand a drastic reduction of the vector mesons masses in medium. Hadronic calculations [10, 11, 12] suggest only marginal changes of the in-medium rho meson mass, but a strongly increased decay width instead. It was shown [12, 13] that this is also in agreement with QCD sum rule analysis if one replaces the delta function by the full spectrum. Taking also p-wave interactions [14] into account this leads to an agreement with the CERES dilepton data.

In a thermal model the dilepton yields of heavy ion collisions are governed by the thermal dilepton rates given by

$$\frac{dR}{d^4x d^4q} = -\frac{\alpha^2}{\pi^3 q^2} \text{Im} \Pi(q, \rho, T) f_B(q, T), \quad (1)$$

with $\alpha = e^2/4\pi = 1/137$. We denote the four-momentum of the dilepton pair by q , the temperature and the density of the system with T and ρ . The space-time volume element which radiates the dilepton pair is d^4x . Apart from the trivial Boltzmann factor f_B , only the imaginary part of the current-current correlation function $\Pi(q, \rho, T)$, which we will investigate in this talk, determines directly the dilepton rates.

In section 2 we review the properties of the current-current correlation function in the vacuum. The corresponding correlation functions in baryonic matter will be developed in section 3. To leading order in the density this requires a detailed calculation of the vector meson-nucleon scattering amplitudes. The in-medium spectra and their comparison with QCD sum rules will then be presented in chapter 4. In section 5 we compare the resulting dilepton rates with the CERES data. We also show the result from the correlation function which originates from uncorrelated quark-antiquark pairs. We will see that both scenarios agree with present data. We therefore suggest to study vector mesons in additional experiments under more moderate conditions, such as the $A(d, {}^3He)$ pick-up reaction, to gain further informations.

2 Vector mesons in the vacuum

Before we start looking into the in-medium properties of neutral vector mesons it is useful to give a brief reminder of their vacuum properties. Since the vector mesons are not stable they can only be seen as resonances in the current-current (CC) correlation function,

$$\Pi_{\mu\nu}(q) = i \int d^4x e^{iq\cdot x} \langle 0 | \mathcal{T} j_\mu(x) j_\nu(0) | 0 \rangle, \quad (2)$$

where \mathcal{T} denotes the time-ordered product and j_μ is the electromagnetic current. It can be decomposed as

$$j_\mu = j_\mu^\rho + j_\mu^\omega + j_\mu^\phi \quad (3)$$

into vector currents specified by their quark content:

$$j_\mu^\rho = \frac{1}{2}(\bar{u}\gamma_\mu u - \bar{d}\gamma_\mu d), \quad (4)$$

$$j_\mu^\omega = \frac{1}{6}(\bar{u}\gamma_\mu u + \bar{d}\gamma_\mu d), \quad (5)$$

$$j_\mu^\phi = -\frac{1}{3}(\bar{s}\gamma_\mu s). \quad (6)$$

Current conservation implies a transverse tensor structure

$$\Pi_{\mu\nu}(q) = \left(g_{\mu\nu} - \frac{q_\mu q_\nu}{q^2} \right) \Pi(q^2), \quad (7)$$

with the scalar CC correlation function

$$\Pi(q^2) = \frac{1}{3}g^{\mu\nu}\Pi_{\mu\nu}(q). \quad (8)$$

The imaginary part of the correlation function is proportional to the cross section for $e^+e^- \rightarrow \text{hadrons}$:

$$R(s) = \frac{\sigma(e^+e^- \rightarrow \text{hadrons})}{\sigma(e^+e^- \rightarrow \mu^+\mu^-)} = -\frac{12\pi}{s} \text{Im}\Pi(s) \quad (9)$$

where $\sigma(e^+e^- \rightarrow \mu^+\mu^-) = 4\pi\alpha^2/3s$ with $\alpha = e^2/4\pi = 1/137$. The vector mesons can be distinguished by looking at different hadronic channels with corresponding flavour (isospin) quantum numbers. We show for example the isovector current describing the ρ meson. G-parity demands that it decays only into even numbers of pions (see data in fig.1a). We observe two different energy regions: the low energy region of the CC correlation function is very well

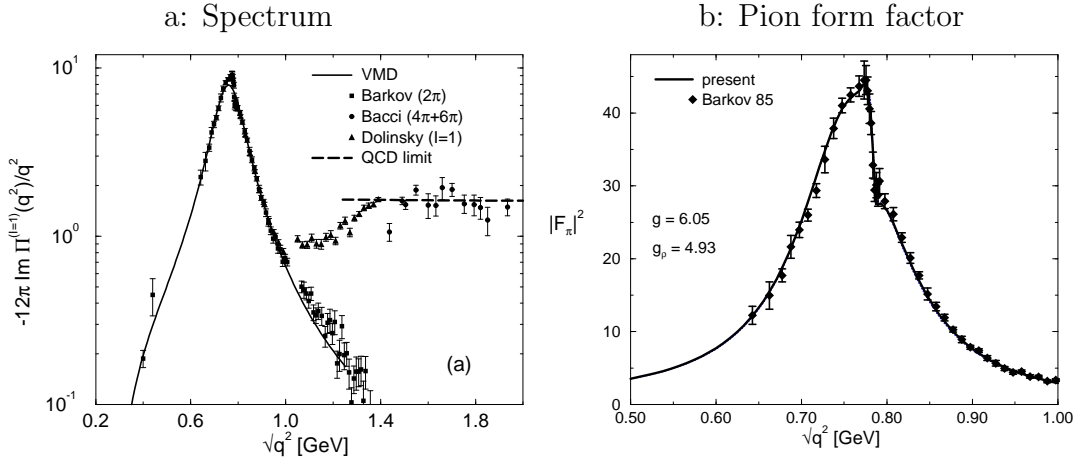


Figure 1: Spectrum of the isovector current-current correlation function in the vacuum and the pion form factor. The solid lines shows result from our vector meson dominance calculation [15].

described by a hadronic language through vector meson dominance (VMD). The extended VMD model [15] gives

$$\text{Im}\Pi^{(I=1)}(q^2) = \frac{\text{Im}\Pi_\rho^{\text{vac}}(q^2)}{g^2} |F_\pi(q^2)|^2, \quad (10)$$

which is shown by the solid line in Fig 1a. It is determined by the imaginary part of the vacuum ρ -meson self energy Π_ρ^{vac} [15], which comes from the decay of the ρ into two pions, and the pion form factor

$$F_\pi(q^2) = \frac{\left(1 - \frac{g}{g_\rho}\right) q^2 - \overset{\circ}{m}_\rho^2}{q^2 - \overset{\circ}{m}_\rho^2 - \Pi_\rho(q^2)}, \quad (11)$$

shown in fig 1b explicitly. Here $\overset{\circ}{m}_\rho$ is the bare ρ meson mass and g (g_ρ) is the coupling of the ρ meson to the pion (photon). The ratio of g to g_ρ is identical to unity in case of “complete” VMD in which all of the hadronic electromagnetic interaction is transmitted through vector mesons. Note in passing that the denominator of the pion form factor is the full ρ meson propagator, which originates from the intermediate ρ -meson as depicted in fig.2 and gives rise to the peak in the pion form factor at the rho meson mass. Isospin violating processes are small but visible as $\rho\omega$ mixing corrections in the peak of the pion formfactor (see Fig 1b).

In the high energy region on the other hand the measured correlation function approaches the asymptotic plateau predicted by perturbative QCD:

$$-\frac{12\pi}{q^2} \text{Im}\Pi(q^2) = \frac{3}{2} \left(1 + \frac{\alpha_S}{\pi}\right) \Theta(q^2 - s_0) \quad (12)$$

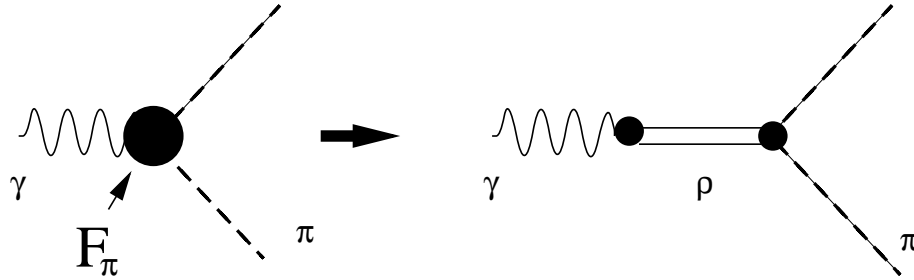


Figure 2: Diagrammatic resolution of the pion form factor

The threshold s_0 lies at about 1.2 GeV^2 . This continuum stems from a picture where the photon couples directly to a quark-antiquark pair, which travels freely over a short distance and then hadronizes into the multi pion continuum. Note that a system of uncorrelated quark and gluons ("Quark-Gluon-Plasma") would also lead to such a plateau in the spectrum. The threshold would then start already at twice the current quark mass.

3 Current correlation functions in baryonic matter

The CC-correlation function in medium at temperature $T = 0$ is defined as

$$\Pi_{\mu\nu}(\omega, \vec{q}; \rho) = i \int_{-\infty}^{+\infty} dt \int d^3x e^{i\omega t - i\vec{q} \cdot \vec{x}} * \langle \rho | \mathcal{T} j_\mu(t, \vec{x}) j_\nu(0) | \rho \rangle, \quad (13)$$

where we have replaced the vacuum by $|\rho\rangle$, the ground state of infinite, isotropic and isospin symmetric nuclear matter with density ρ . We assume matter as a whole to be at rest. This specifies the Lorentz frame that we will use in the following. For $\vec{q} = 0$, the case where the vector meson is at rest, only the transverse tensor structure survives and $\Pi^{00} = \Pi^{0j} = \Pi^{i0} = 0$. We write

$$\Pi_{ij}(\omega, \vec{q} = 0; \rho) = -\delta_{ij} \Pi(\omega, \vec{q} = 0; \rho). \quad (14)$$

As a first step we apply the low density theorem [16] to the self energy of the vector mesons:

$$\Pi_V(\omega, \vec{q} = 0; \rho) = \Pi_V^{\text{vac}}(\omega^2) - \rho T_{VN}(\omega) + \dots, \quad (15)$$

where T_{VN} is the vector meson-nucleon scattering amplitude taken at $\vec{q} = 0$. We can extend eq.(10) to the in-medium correlation function in terms of VMD and write [12]

$$\begin{aligned} \text{Im} \Pi(\omega, \vec{q} = 0; \rho) &= \frac{1}{g_V^2} \text{Im} \left(\Pi_V^{\text{vac}}(\omega^2) - \rho T_{VN}(\omega) \right) \\ &* \left| \frac{(1 - a_V) \omega^2 - \overset{\circ}{m}_V^2}{\omega^2 - \overset{\circ}{m}_V^2 - (\Pi_V^{\text{vac}}(\omega^2) - \rho T_{VN}(\omega))} \right|^2. \end{aligned} \quad (16)$$

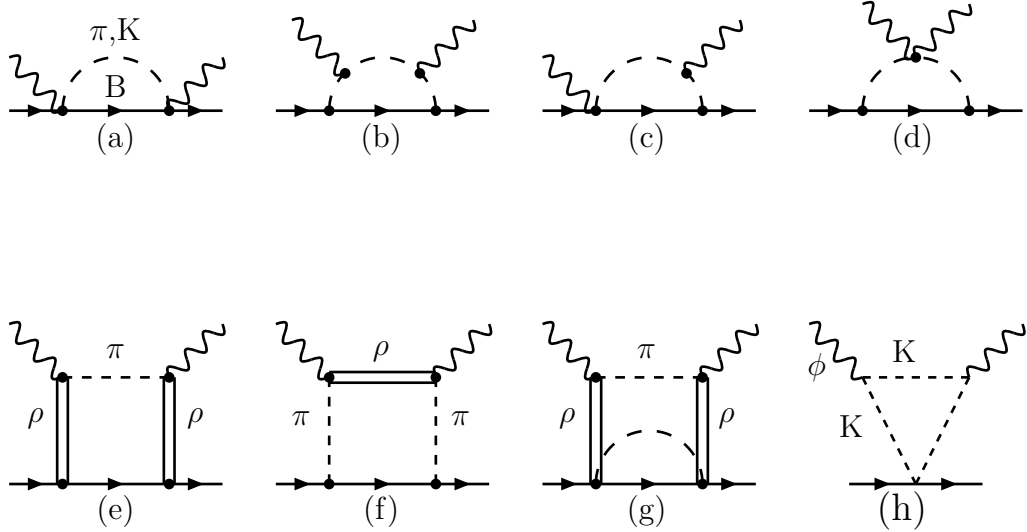


Figure 3: Dominant diagrams for the Compton amplitude $T(\omega)$ and the vector meson-nucleon amplitudes $T_{VN}(\omega)$. In order to get from T to T_{VN} , replace the (wavy) photon line by the relevant vector mesons. Diagrams (e) and (f) operate, in particular, in the ω meson channel.

We wrote down here the general form for all three channels replacing g by g_V and denoting the ratio by a_V . The vacuum vector meson self energy was replaced by eq.(15) which includes the complete set of medium modifications. In order to determine the in-medium correlation function we are left with the task to calculate the vector meson-nucleon scattering amplitudes. We use an effective Lagrangian which combines chiral SU(3) dynamics with VMD. This Lagrangian has been applied successfully in the vacuum [15] and has been extended to incorporate meson-baryon interactions. For the baryons we include the complete baryon octet and decuplet (nucleons, hyperons, Δ 's, etc.).

The most important processes contributing to the scattering amplitudes are shown in fig.3 for the ρ , ω and ϕ meson respectively. For the ρ (ϕ) meson we draw the diagrams which survive in the limit of large baryon mass (fig. 3a-d). The last one (fig. 3d) only contributes to the real part of the ρN (ϕN) scattering amplitude. While for the ρ -meson the πN and $\pi \Delta$ loops govern the scattering amplitude, $K\Sigma$, $K\Lambda$ and $K\Sigma(1385)$ loops dominate for the ϕ meson. We also include s-wave scattering of the kaons (fig. 3h) [17]. For the ωN scattering amplitude we only show the dominant contributions to the imaginary part (figs. 3e, f, g). We evaluate the imaginary parts of the amplitudes by cutting the diagrams in all possible ways. The real parts are then determined by using a once subtracted dispersion relation, with the subtraction constant fixed by the Thomson limit. Evaluating those diagrams and using eq.(16) we plot the spectra of the correlation functions for various

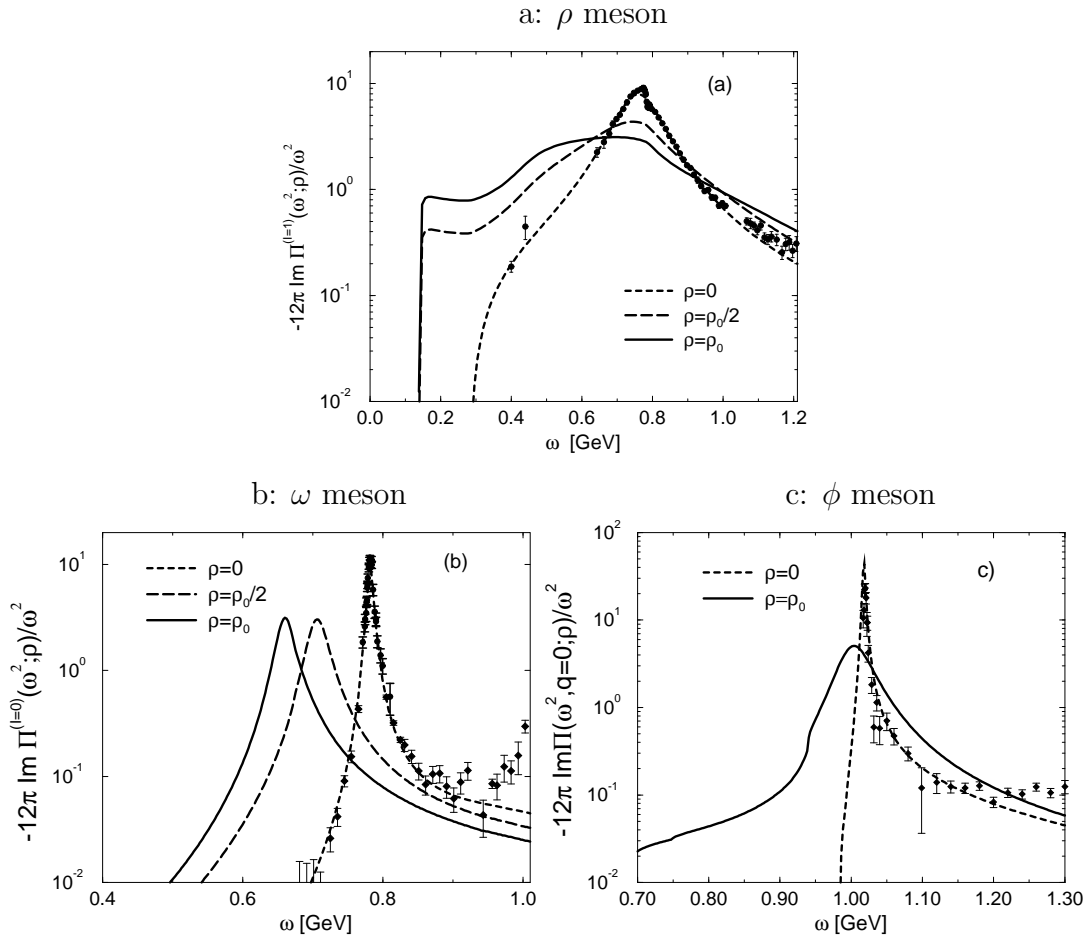


Figure 4: Calculated spectra of current-current correlation functions. The dashed lines show the vacuum spectra in the ρ , ω and ϕ channels normalized such that they can be compared directly with the corresponding $e^+e^- \rightarrow$ hadrons data. The long dashed and solid lines show the spectral functions in nuclear matter at densities $\rho_0/2$ and $\rho_0 = 0.17 \text{ fm}^{-3}$, as discussed in section 3.

densities as shown by the curves in fig. 4a, b and c. We observe important differences between the various channels. The ρ meson mass decreases only slightly while the width increases very strongly. This causes the peak to shift downwards and broaden. We also see strong threshold contributions starting at the pion mass. The ρ -meson therefore dissolves in nuclear matter; it is not a good quasi-particle any longer. On the other hand the mass of the ω meson decreases significantly. Its width also increases but not as strongly as for the ρ meson and so it can still be regarded as a good-quasi particle. For the ϕ meson there is almost no change in the peak position while the width increases.

4 Comparison with QCD sum rules

Up to now we only looked at the time like region of the correlation function where it has an imaginary part and is therefore experimentally accessible. Now we want to concentrate on the spacelike region. For momentum $|q^2| \gg 1 \text{ GeV}$ the correlation function is governed by perturbative QCD which is well under control. The interesting region is the space like region at around $Q^2 = -q^2 \simeq 1 \text{ GeV}$ where non-perturbative effect start to become important. The basic idea of QCD sum rules [18] is to compare two ways of determining $\Pi(q^2)$ in this region. One way is to use a twice subtracted dispersion relation for each one of the channels $V = \rho, \omega, \phi$:

$$\Pi(q^2) = \Pi(0) + c q^2 + \frac{q^4}{\pi} \int ds \frac{\text{Im}\Pi(s)}{s^2(s - q^2 - i\epsilon)}, \quad (17)$$

where one uses the measured or calculated spectrum $\text{Im}\Pi$ in the time-like region as input. The other one is to calculate the correlation function using the operator product expansion (OPE):

$$\begin{aligned} \frac{12\pi}{Q^2} \Pi(q^2 = -Q^2) = & \frac{d}{\pi} \left[-(1 + \alpha_S(Q^2)/\pi) \ln \left(\frac{Q^2}{\mu^2} \right) \right. \\ & \left. + \frac{c_1}{Q^2} + \frac{c_2}{Q^4} + \frac{c_3}{Q^6} + \dots \right]. \end{aligned} \quad (18)$$

Here d agrees with the value of the perturbative continuum (e.g. $d=3/2$ for the isovector channel) and the coefficients $c_{1,2,3}$ incorporate the non-perturbative parts coming from the condensates such as the gluon condensate in c_2 or the four-quark condensate in c_3 . In medium these coefficients become density dependent because the condensates change in matter and new condensates arise. We use the values $c_2^{\rho,\omega} = 0.04 + 0.018(\rho/\rho_0) \text{ GeV}^4$ and $c_3^{\rho,\omega} = -0.07 + 0.036(\rho/\rho_0) \text{ GeV}^6$ proposed by Hatsuda et al. [9] for the ρ and ω meson. They neglected higher twist condensates which are hardly known but might be important. For the four-quark condensates we assume as in ref.[9] that ground state saturation holds to the same extent as in the vacuum. The coefficient c_1 is proportional to the squared quark mass; due to the small mass of the up and down quark we can safely neglect those contributions and set $c_1^{\rho,\omega} = 0$. The situation is different in case of the ϕ meson. Because of the large strange quark mass c_1 is no longer negligible and we take the values $c_1^\phi = -0.07 \text{ GeV}^2$, $c_2^\phi = -0.1 + 0.01(\rho/\rho_0) \text{ GeV}^4$ and $c_3^\phi = -0.07 + 0.006(\rho/\rho_0) \text{ GeV}^6$.

A Borel transform is used in order to improve the convergence of the OPE series. Comparing eq.(17) and (18) after Borel transformation we end up with

$$\begin{aligned} \frac{12\pi^2\Pi(0)}{d\mathcal{M}^2} + \frac{1}{d\mathcal{M}^2} \int_0^\infty ds R(s) \exp \left[-\frac{s}{\mathcal{M}^2} \right] = \\ (1 + \alpha_S(\mathcal{M}^2)/\pi) + \frac{c_1}{\mathcal{M}^2} + \frac{c_2}{\mathcal{M}^4} + \frac{c_3}{2\mathcal{M}^6}, \end{aligned} \quad (19)$$

where the Borel mass parameter should be chosen in the range $\mathcal{M} \gtrsim 1$ GeV in order to ensure convergence of the OPE side of eq.(19). The “left side” comes from the dispersion relation of eq.(17) and R represents the ratio (9), but now specified for each individual flavour channel with $V = \rho, \omega, \phi$. The “right side” is determined by the OPE. In fig. 3a, b and c we show the comparison between the “left side” (solid line) and the “right side” (dashed line) for the various channels. The consistency between “left” and “right” sides in the vacuum is evidently quite satisfactory. Only for a Borel mass below 0.8 GeV higher order terms in the OPE become important and the convergence fails. The agreement at normal nuclear matter density is not as excellent as in the vacuum but still very impressive. We therefore conclude that QCD sum rules and our hadronic model of the in-medium current-current correlation function are mutually compatible. We also point out that assuming a simple pole ansatz for the spectrum at finite densities can lead to erroneous interpretation of the in-medium masses. This is very obvious in the isovector channel. While our model gives only a small change of the rho mass a simple pole ansatz leads to a reduction of m_ρ by more than 10 percent [9] at $\rho = \rho_0$.

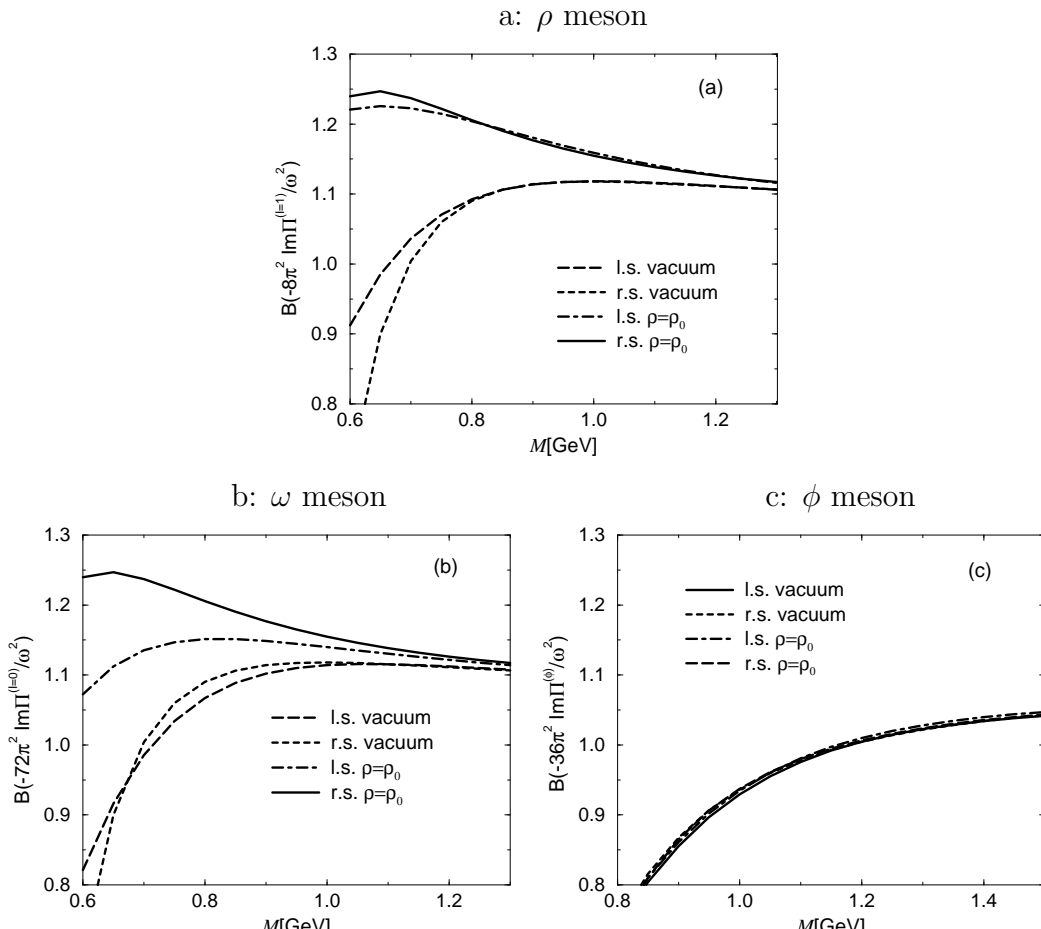


Figure 5: Comparison of the “left” and “right” side of the QCD sum rules (15) in the vacuum (solid and dashed line) and at normal nuclear density (dot dashed and long dashed line) as a function of the Borel mass parameter M .

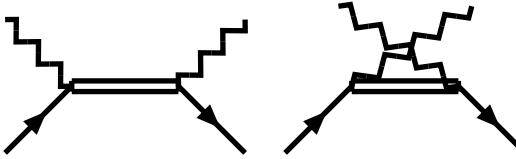


Figure 6: The Isobar model for the p-wave interaction of the ρ -meson (wavy-line) with the nucleons (solid line). The double line are the resonances, where explicitly include the $\Delta(1232)$, $N^*(1720)$ and $\Delta^*(1905)$.

5 Can one observe chiral restoration?

We now want to compare our result of the correlation function with the dilepton data measured by CERES [5]. Since the dileptons at this high energy collisions carry momenta which are of the same order as their invariant mass, we also have to include the p-wave modification of the correlation function. Friman and Pirner [14] used an isobar model shown in fig. 6 in order to take the p-wave interaction of the ρ -meson with the nucleons into account. They include in particular the $N^*(1720)$ and the $\Delta^*(1905)$ resonance. For the other vector mesons no such resonances are known. This gives rise to a momentum dependent vector meson-nucleon scattering amplitude $T_{VN}(\omega, \vec{q})$ which we also include in eq.(16). Under the assumption that the change of the spectrum is mainly due to the density, we can use the resulting $\text{Im } \Pi(q, \rho, T = 0)$ as input for eq.(1) and determine the thermal dilepton rates. Integrating this over the different momenta of the dileptons, the volume $V(t) = N_B/\rho(t)$ and the time evolution of the fireball, we are able to estimate the rate of dilepton pairs emitted in a heavy ion collision of sulfur on gold at CERN:

$$\frac{d^2 N_{e^+e^-}}{d\eta dm_{e^+e^-}} = \int_0^{t_f} dt V(t) \int d^3 q \frac{m_{e^+e^-}}{q_0} \cdot \frac{dR(q, \rho(t), T(t))}{d^4 x d^4 q} A(q). \quad (20)$$

where $A(q)$ is the acceptance of the CERES detector. Now we just have to assume a suitable density and temperature profile which we adapt from the usual transport code calculations [19]:

$$T(t) = (T^i - T^\infty) e^{-t/\tau_1} + T^\infty \quad (21)$$

with an initial temperature $T^i = 170$ MeV. For the final temperature we take $T^\infty = 110$ MeV and we use $\tau_1 = 8$ fm. For the density profile we use

$$\rho(t) = \rho_i \exp(-t/\tau_2); \quad (22)$$

with $\rho_i = 2.5\rho_0$ and $\tau_2 = 5$ fm. We show the result in fig.7a and compare it with the case where we use the free spectrum at $\rho = 0$. One clearly observes a strong improvement as compared to the free case.

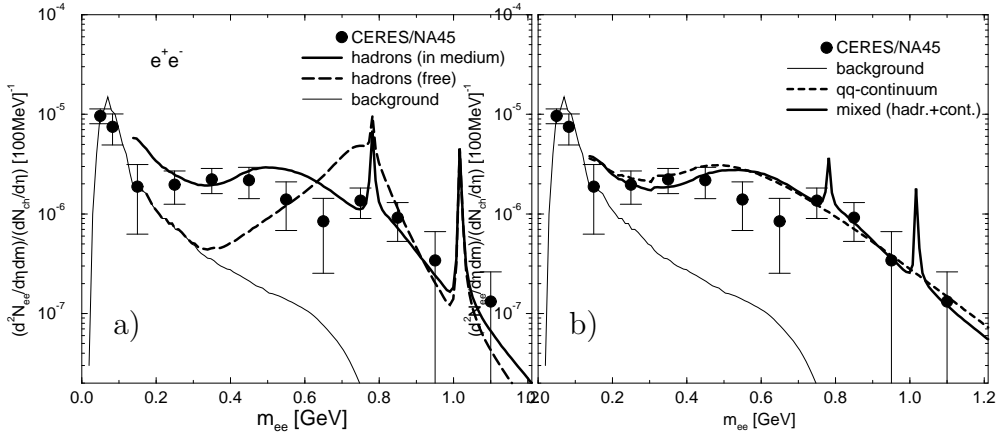


Figure 7: Comparison of the dilepton rates from sulfur on gold collisions measured by the CERES collaboration [5] with
a)a hadronic system assuming medium or vacuum properties
b)a system of uncorrelated quark and gluons or a mixed system of this and a hadronic phase.

Now we want to study whether chiral restoration might already occur in such collisions and assume, as an extreme limit, as system of free, uncorrelated quarks and gluons. Then the spectrum of the correlation function would have the constant value of the perturbative plateau in eq.(12). We therefore assume $-12\pi/q^2 \text{Im}\Pi(q^2) = 5/3$ below the strange quark threshold and 2 above. The result is shown in fig.7b using otherwise the same temperature and baryon density profile as in the hadronic case. The consistency with the data is astonishing. It is clear, however, that in a realistic scenario both hadronic and quark-gluon phases must be present. If the initial fireball temperature is as large as $T^i = 170 \text{ MeV}$, the system should have already a substantial quark-gluon component. We therefore assume next that the uncorrelated quarks exist at temperatures above 140 MeV. Below that temperature, the hadronic scenario sets in. The result is also shown in fig.7b.

Considering roughly comparable magnitudes of dileptons produced in both, the hadronic scenario and the phase of uncorrelated quark and gluons, the real problem is how one can distinguish them. It is clear that at the moment the precision of the CERES data opens no way to separate them. A possible signal might be the suppression of the ω - and ϕ -meson peak in the quark-gluon phase. But also a strong broadening of these resonances in the hadronic phase can lead to a similar suppression. It is therefore essential first to study the hadronic properties more precisely, and under more moderate conditions.

One way is to look for bound ω -meson states. In our hadronic model

for example we observe a strong attractive potential for the ω -meson in nuclear matter. This behaviour is also supported by QCD sum rules. Such an attractive potential would lead to bound ω meson states already in a light nucleus like Lithium. Such states could be produced via a transfer reaction like $d + A \rightarrow {}^3He + (A - 1) + \omega$ [20]. Here the incoming deuteron d picks up one proton from the target nucleus A and is detected as 3He in forward direction. During this process the ω -meson is produced and possibly bound in the residual $(A - 1)$ -nucleus. The preferred deuteron beam energy is such that the ω is produced with minimal possible momentum. The momentum and energy conservation determines then the energy of the bound ω -meson. A typical spectrum which one expects on the basis of a realistic distorted wave Green's functions calculation, is shown in Fig.8. We recognize that the

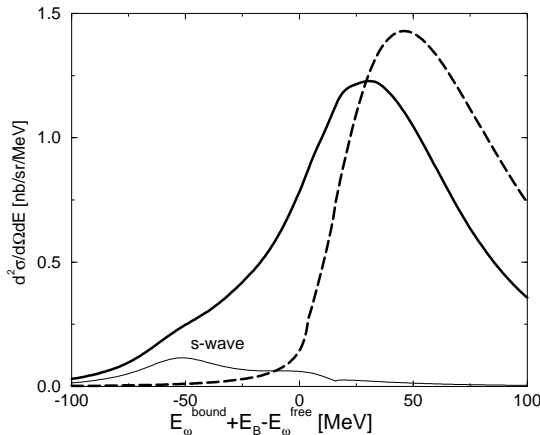


Figure 8: Typical spectrum of the transfer reaction $d + A \rightarrow {}^3He + (A - 1) + \omega$. We consider the results from the free potential (dashed line) and from our in-medium potential (solid line)

increased medium width broadens the single bound ω strongly and makes it difficult to identify separate levels. Nevertheless, one would expect to observe a strong downward shift of the spectral weight which would be a signal for an attractive medium potential. Of course, the differential cross section for this process is small, and a detailed examination of competing background (not taken into account in Fig. 8) is necessary.

6 Conclusions

We have compared the dilepton rates arising from a hadronic model with those coming from a phase of uncorrelated quarks. Both scenarios describe the CERES-data well and can not be distinguished at the present level of accuracy. More precise data under less extreme thermodynamic conditions are needed, e.g. from the forthcoming HADES experiments at GSI which permit

better e^+e^- resolution. One should also study the possibility of bound states of ω -mesons in order to gain more information and better understanding.

References

- [1] T.D. Cohen, R.J. Furnstahl and D.K. Griegel, Phys. Rev. **C 45**(1992)1881.
- [2] J. Engels, F. Karsch and K. Redlich, Nucl. Phys. **B 435** (1995) 295.
- [3] G. Boyd et al., Phys. Rev Lett. **75**(1995) 295.
- [4] M. Lutz, S. Klimt and W. Weise, Nucl. Phys. **A 542** (1992) 521.
- [5] G. Agakichiev et al., Phys. Rev. Lett. **75** (1995) 1272.
- [6] M. Masera et al., Nucl. Phys. **A 590** (1995) 93c.
- [7] G.E. Brown and M. Rho, Phys. Rev. Lett. **66** (1991) 2720.
- [8] K. Saito and A.W. Thomas, Phys. Rev. **C 52** (1995) 2789.
- [9] T. Hatsuda and S.H. Lee, Phys. Rev. **C 46** (1992) R34.
- [10] M. Herrmann, B.L. Friman and W. Nörenberg, Nucl. Phys. **A 560** (1993) 411.
- [11] G. Chanfray and P. Schuck, Nucl. Phys. **A 555** (1993) 329.
- [12] F. Klingl, N. Kaiser and W. Weise, Nucl. Phys. **A 624** (1997) 527.
- [13] S. Leupold, W. Peters and U. Mosel, nucl-th/9708016.
- [14] B. Friman and H.J. Pirner, Nucl. Phys. **A 617** (1997) 496.
- [15] F. Klingl, N. Kaiser and W. Weise, Z. Phys. **A 356** (1996) 193.
- [16] C.D. Dover, J. Hüfner and R.H. Lemmer, Ann. Phys **66** (1971) 248.
- [17] F. Klingl, T. Waas and W. Weise, hep-ph/9709210, subm. to Phys. Lett. **B**(1997).
- [18] M.A. Shifman, A.I. Vainshtein and V.I. Zakharov, Nucl. Phys. **B 147** (1979) 385.
- [19] R. Rapp, G. Chanfray and J. Wambach, Nucl. Phys. **A 617** (1997) 472.
- [20] A. Gillitzer, R.S. Hayano et al., GSI-Proposal # S214.